EUROPEAN FUSION DEVELOPMENT AGREEMENT

EFDA–JET–CP(01)02-07

J. Ongena, W. Suttrop, M. Bécoulet, G. Cordey, P. Dumortier, Th. Eich, L.C. Ingesson, S. Jachmich, P. Lang, A. Loarte, P. Lomas, G.P. Maddison, A. Messiaen, M.F.F. Nave, J. Rapp, G. Saibene, R. Sartori, O. Sauter, J.D. Strachan, B. Unterberg, M. Valovic, B. Alper, Ph. Andrew, Y. Baranov, J. Brzozowski, J. Bucalossi, M. Brix, R. Budny, M. Charlet, I. Coffey, M. De Baar, P. De Vries, C. Gowers, N. Hawkes, M. von Hellermann, D.L. Hillis, J. Hogan, G.L. Jackson, E. Joffrin, C. Jupen, A. Kallenbach, H.R. Koslowski, K.D.Lawson, M.Mantsinen, G. Matthews, P. Monier-Garbet, D. McDonald, F. Milani, M. Murakami, A. Murari, R. Neu, V. Parail, S. Podda, M.E. Puiatti, E. Righi, F.Sartori, Y.Sarazin, A.Staebler, M.Stamp, G.Telesca, M.Valisa, B.Weyssow, K-D. Zastrow
and JET EFDA Contributors

Recent Progress on JET Towards the ITER Reference Mode of Operation at High Density

Recent Progress on JET Towards the ITER Reference Mode of Operation at High Density

J. Ongena[1+], W. Suttrop[2], M. Bécoulet[3], G. Cordey[4], P. Dumortier[1], Th. Eich[5], L.C. Ingesson[6], S. Jachmich[1], P. Lang[5], A. Loarte[7], P. Lomas[4], G.P. Maddison[4], A. Messiaen[1], M.F.F. Nave[8], J. Rapp[5], G. Saibene[7], R. Sartori[7], O. Sauter[9], J.D. Strachan[10], B. Unterberg[5], M. Valovic[4], B. Alper[4], Ph. Andrew[4], Y. Baranov[4], J. Brzozowski[10], J. Bucalossi[3], M. Brix[5], R. Budny[11], M. Charlet[4], I. Coffey[4], M. De Baar[6], P. De Vries[6], C. Gowers[4], N. Hawkes[4], M. von Hellermann[6], D.L. Hillis[12], J. Hogan[12], G.L. Jackson[13], E. Joffrin[3], C. Jupen[10], A. Kallenbach[2], H.R. Koslowski[5], K.D.Lawson[4], M.Mantsinen[4], G. Matthews[4], P. Monier-Garbet[3], D. McDonald[4], F. Milani[4], M. Murakami[12, 13], A. Murari[14], R. Neu[2], V. Parail[4], S. Podda[14], M.E. Puiatti[15], E. Righi[7], F.Sartori[4], Y.Sarazin[3], A.Staebler[2], M.Stamp[4], G.Telesca[15], M.Valisa[15], B.Weyssow[16], K-D. Zastrow[4]
and JET EFDA Contributors*

[1]*LPP / ERM-KMS, Association EURATOM-Belgian State, B-1000 Brussels, Belgium†*
[2]*Max-Planck Institut für Plasmaphysik, EURATOM Association, D-85748 Garching, Germany*
[3]*CEA Cadarache, F-13108 St Paul lez Durance, France*
[4]*EURATOM/UKAEA Fusion Association, Culham, UK*
[5]*Institut für Plasmaphysik, Forschungszentrum Jülich GmbH, EURATOM Association, D-52425 Jülich, Germany†*
[6]*FOM-Instituut voor Plasmafysica, EURATOM Association, Postbus 1207, NL-3430 BE Nieuwegein, Netherlands†*
[7]*EFDA-Close Support Unit, D-85748 Garching, Germany*
[8]*Centro de Fusão Nuclear, Association "EURATOM-IST, 1096 Lisbon, Portugal*
[9]*Centre de Recherches en Physique des Plasmas, Ecole Polytechnique de Lausanne, Association "EURATOM-Confederation Suisse", Lausanne, Switzerland.*
[10]*Chalmers University of Technology, Association "EURATOM-NFR", Göteborg, Sweden*
[11]*Princeton Plasma Physics Laboratory, Princeton University, NJ 08543, USA*
[12]*Oak Ridge National Laboratory, Oak Ridge, TN 37831, USA*
[13]*DIII-D National Fusion Facility, San Diego, CA 92186-5698, USA*
[14]*Associazione EURATOM-ENEA sulla Fusione, Centro Ricerche Frascati, C.P. 65, 00044-Frascati (Rome), Italy*
[15]*Consorzio RFX - Associazione Euratom-Enea sulla Fusione, Corso Stati Uniti 4, I-35127 Padova, Italy*
[16]*Université Libre de Bruxelles, Association "EURATOM-Belgian State", Physique Théorique et Mathématique, Unité de Physique des Plasmas, 1050 Brussels.*
[+]*Researcher at NFSR Belgium*
[†]*Partners in the Trilateral Euregio Cluster (TEC)*
**See appendix of the paper by J.Pamela "Overview of recent JET results", Proceedings of the IAEA conference on Fusion Energy, Sorrento 2000*

Preprint of Paper to be submitted for publication in Proceedings of the EPS Conference,(Madeira, Portugal 18-22 June 2001)

ABSTRACT

Recent progress is summarized towards obtaining high density and high confinement in JET as required for the ITER reference scenario at Q=10. Plasmas with simultaneously confinement $H_{98(y,2)}$=1 and densities up to n/n_{GW} ~1 are now routinely obtained. This has been possible (i) using plasmas at high (δ~0.5) and medium (δ~0.3-0.4) triangularity with sufficient heating power to maintain Type I ELMs (ii) with impurity seeded plasmas at high (δ~0.5) and low (δ≤0.2) triangularity (iii) with an optimised pellet injection sequence, keeping energy confinement and raising the density and (iv) by carefully tuning the gas puff rate leading to plasmas with peaked density profiles and good confinement at long time scales. These high performance discharges exhibit Type I ELMs, with a new and more favourable behaviour observed at high densities, requiring further studies. Techniques for a possible mitigation of these ELMs are discussed, and first promising results are obtained with impurity seeding in discharges at high triangularity. Scaling studies using the new data of this year show a strong dependence of confinement on the upper triangularity, the density and the proximity to the Greenwald limit. MHD instabilities observed and methods to avoid these in high density and high confinement plasmas are discussed.

1. INTRODUCTION

The ITER reference operational scenario is the ELMy H-Mode with a confinement quality $H_{98(y,2)}$=1 and beta value β_N=1.8 at a density normalized to the Greenwald density [1] n/n_{GW}=0.85 (with n_{GW} $[10^{20}m^{-3}] = I_p$ [MA]/($\pi a^2[m^2]$). Previous experiments in JET and other tokamaks have shown that it becomes increasingly more difficult to keep good confinement properties in the ELMy H-Mode at higher densities, usually obtained by gas puff. This year, however, discharges have been obtained at JET with simultaneous high 3 density and high confinement using several techniques : (i) by increasing the triangularity of the plasma to high values δ~0.5, (ii) at medium triangularities δ~0.3-0.4 by increasing the additional heating power such as to keep Type I ELMs (iii) by impurity seeding in plasmas with both high and low triangularity (iv) by fuelling the plasma with an optimised pellet injection sequence and (v) by carefully tuning the gas input, leading to density peaking and densities around or above the Greenwald factor on long time scales. Using these methods or combinations confinement and density requirements have been reached and in some cases even surpassed for the Q=10 ITER reference scenario [2] during quasi-stationary periods of up to 6 seconds or up to $15\times\tau_E$, a duration which was limited by the designed pulse length capabilities of JET. These long pulse high performance discharges exhibit Type I ELMs, and it is another challenge to mitigate the effect of ELMs, in order to avoid excessive erosion or sputtering of the first wall. Several techniques for ELM mitigation have been studied with and without impurity radiation, and first results indicate possible promising routes to the realisation of an operational scenario for ITER that is combining high performance with an acceptable heat exhaust. A significant influence is found of the triangularity, the density peaking and the proximity to the Greenwald density on the scaling of the energy confinement. It is the purpose of this paper to summarize the

main results of experiments undertaken this year on JET aimed at obtaining simultaneous high confinement and high density in view of ITER.

2. HIGH DENSITY AND HIGH CONFINEMENT IN HIGHLY SHAPED PLASMAS

Recent experiments on ASDEX, DIII-D, JET and JT-60 [3-7] have shown the positive influence of triangularity on confinement. This year, the upper and lower triangularity of the plasma, δ_U and δ_L, have been varied independently in JET to study the influence of these parameters on plasma confinement. A large number of different plasma shapes have been tested. One of them is the so called "ITER-like" shape (elongation κ=1.74 and average triangularity $\delta=(\delta_U + \delta_L)/2 \sim 0.45$-$0.5$). The working gas of the discharges is deuterium with a few percent (~2-3%) of hydrogen. In what follows the ratio P_{heat}/P_{L-H} of the additional heating power to the L-H threshold power will be used as a convenient way to quantify the power level used, as discussed in Ref. [8]. ITER-like plasmas (Fig. 1), simultaneously realise high density up to $n/n_{GW} = 1$ with slight peaking ($\bar{n}$-/n_{ped} = 1.2-1.3, where n- is the line average over a central chord (R=3.02m) and n_{ped} is the line average over a chord in the edge region (R=3.75m)), high confinement $H_{98(y,2)} \sim 1$ (with $H_{98(y,2)}$ the enhancement factor over ELMy H-Mode as given by the IPB98-P(y,2) scaling expression [2]), and high normalized beta $\beta_N = 2$ for quasistationary time intervals lasting several seconds (more than 6s for the discharge of Fig. 1). This duration is close to the maximum technically realizable flattop time in JET for this operational scenario. To obtain good confinement conditions in high triangularity scenarios, in addition attention has to be paid to avoid large first ELMs. This was done using gas puffs in the beginning of the discharge. The idea was to keep the size of the first ELM below the level that creates seed islands for Neoclassical Tearing Modes (NTM) as mode numbers m/n=3/2 are often observed after large ELMs.

Typically, such plasmas have low frequency Type I ELMs [9]. At all triangularities there is a confinement degradation with density but higher triangularities achieve higher densities with good confinement (Fig. 2). Data from ITER-like plasmas encompass now the ITER design point ($\bar{n}\, n_{GW}$ / = 0.85 and $H_{98(y,2)} = 1$).

High confinement was also obtained with strong gas puff in lower triangularity plasmas (δ~0.3) by increasing the heating power sufficiently to maintain Type I ELMs. This was done for two sets of discharges (Fig. 3) at medium triangularity (δ=0.33) at low and high values for P_{heat}/P_{L-H} ($1.6 < P_{heat}/P_{L-H} < 2.1$ and $2.4 < P_{heat}/P_{L-H} < 4.2$). The higher values for P_{heat}/P_{L-H} maintained higher confinement, even with strong gas puff (leading to high densities up to the Greenwald limit) while lower P_{heat}/P_{L-H} led to a degradation of confinement with high gas puff rates, as illustrated in Fig. 3. The confinement degradation is correlated with a change from Type I to Type III ELMs and only densities below the Greenwald limit are reached.

Although the high density in these plasmas was reached by high gas fuelling rates, $H_{98(y,2)}$ degraded by only 5-10%, compared to the unfuelled case. The decreased sensitivity of energy confinement to high gas puff rates of this type of discharges was explained in Ref. [9] in part by a

stabilization of ballooning mode turbulences in the edge due to triangularity. The net result are plasmas with a high stored energy and normalized beta value, high plasma density around the Greenwald limit and consequently low plasma dilution, characterised by a Zeff ~ 1.5.

3. HIGH DENSITY AND HIGH CONFINEMENT IMPURITY SEEDED PLASMAS

Experiments with impurity seeding on TEXTOR, DIII-D, JET and JT-60U [10] have shown that it is possible to combine or even improve the confinement and density properties of plasmas (leading to high confinement, $H_{98(y,2)}$ ~ 1, and high density, n/nGW ~1) with high levels of radiation in the edge. Experiments with radiative mantle plasmas started in JET in 1999 [11] have been continued this year [12-18] in (i) low triangularity discharges with the X-point lowered onto or just inside the material barrier (called septum or dome) dividing the inboard and outboard sides of the divertor, resulting in the so-called "septum" configuration and (ii) discharges at high triangularity with a geometry close to the ITER one.

A. IMPURITY SEEDING IN "SEPTUM" DISCHARGES

This discharge type represents a mid-way between a divertor and pumped limiter configuration. Surprisingly, these discharges have a lower H-Mode threshold power than discharges without septum [19] and thus remain in H-Mode even at high radiation levels. Impurity seeding has been applied to both low (δ=0.2, κ=1.6) and medium triangularity (δ=0.3, κ=1.72) discharges in the septum configuration (Fig. 4). About 0.5s after the application of the additional heating a strong gas puff was applied. Confinement was reduced during the gas puff phase, as seen in the reduction of the enhancement factor $H_{98(y,2)}$ to about 0.8. During the D_2 puff phase, Ar was also puffed and both the radiative power level and plasma density increased. After the D_2 gas fuelling valve closed, the density was constant ($\overline{n}/n_{GW}$ ~ 0.9) and the confinement was restored to pre-puff values ($H_{98(y,2)}$ ~ 1), with radiation fractions P_{rad}/P_{tot} around 50%. In this way values are reached for the product $H_{98(y,2)} \times \overline{n}/nGW$ ~ 0.9 at $\overline{n}/n_{GW}$ ~ 0.9, outstanding for low triangularity plasmas. Those values can be maintained stationary for 5 seconds or about $12\tau_E$. This phase (from 20s onwards in Fig. 4) is called the "afterpuff" phase. During the afterpuff phase, gentle Ar and D_2 refuelling was applied keeping the radiation level and the plasma density constant. Only 15-20% of the input power was radiated in the divertor, with about 30% of the input power radiated in the edge of the main plasma chamber. Ar seeding is more adapted to the JET plasma parameters than Ne, as the latter leads for a given radiation level to a higher Z_{eff}.

Note that the electron density increase is not only resulting from the extra electrons provided by the ionization of the seeded Ar and genuine changes must take place in the particle confinement time τ_p, the fuelling efficiency (as defined in [20]) or both in the presence of Ar.

The same technique (puff and afterpuff) was applied in septum discharges at medium triangularity (δ~0.3), leading to similar results. At δ~0.3, higher densities were obtained with D puff only, whereas at δ=0.2 similar densities could only be obtained with additional Ar seeding during the D puff

phase. Both low and high triangularity discharges with impurity seeding showed a peaking of the electron density profile.

The ELM frequency reduced during Ar seeding for a given (high) density and edge pedestal. Consequently smaller time integrated ELM losses occurred. This will be further discussed in Section 7. Nevertheless, fundamental changes in bulk confinement must also take place, as the Ar seeding also correlated with χ_{eff} (calculated by TRANSP [21]) dropping in the core [10]. Such confinement changes have been clearly shown by a doubling of the ion temperature and high neutron rates when applying Ar seeding in LMode plasmas [16]

B. IMPURITY SEEDED ITER-LIKE PLASMAS

Ar seeded ITER-like plasmas (Fig. 5a-b), showed a radiating mantle and P_{rad}/P_{tot} = 60-70%. ICRH has been applied to avoid impurity accumulation (see section C below). Ar seeding correlates with an increase in the plasma density, up to $1.2\times n_{GW}$ (Fig. 5a). Confinement was unchanged in the Ar seeded discharge ($H_{98(y,2)} \sim 1$). Zeff is somewhat increased from ~1.7 to ~2.0. Further optimisation of these discharges is foreseen with respect to the deuterium and Ar refuelling, in order to further increase the stationarity and the product $H_{98(y,2)}\times\bar{n}/n_{GW}$.

Infrared measurements at a fixed location in the inner and outer divertor, (Fig. 5b) showed a reduction in the surface temperature of the divertor target with Ar seeding. The effect is clearly visible in the inner divertor, and even more in the outer divertor, where the base level is dropping from about 500°C to about 100°C and also the maximum temperature spikes due to ELMs are reduced from 1300°C to 600°C [22]. Although these results are from first IR thermographic measurements in such a scenario and further work is needed to consolidate these findings, the result looks promising as a possible technique for ELM mitigation.

C. APPLICATION OF CENTRAL HEATING IN IMPURITY SEEDED PLASMAS TO OPTIMIZE THE IMPURITY CONTENT [14]

Sawteeth play an important role in keeping a low dilution in the plasma centre of impurity seeded plasmas. In ELMy H-Modes without impurity seeding, generally a slow increase in the central safety factor q(0) is seen. With excessive Ar injection rates, the following four effects are observed: (i) further increase in the central q leading to sawteeth disappearance when $q(0) > 1$ followed by impurity accumulation, (ii) an increase in MHD activity [15] which can lead to (iii) a decrease in the energy confinement time and (iv) appearance of ELM free phases. The causality between these effects needs further study, but the current understanding is that the changes in the central part of the q profile induces the others. Central heating is one means to counteract the modifications in the q profile and to keep $q(0) < 1$, in order to keep the sawtooth MHD. At the higher densities reached in these discharges, the energy deposition of the beams becomes flatter and even hollow. Therefore in addition to NBI heating ICRH (H-minority heating) is applied with the resonance layer located on axis, at moderate heating levels (1-2MW) to avoid sawtooth stabilisation by RF induced fast

ions. The central electron temperature increased, and the central q remained below unity (Fig. 5a). As a result, the sawteeth remained and core impurity accumulation did not occur. Note that sawtooth activity reduces the central impurity content without increasing the impurity content in the rest of the plasma, as deduced from Ar concentration and Zeff profiles.

A $H_{98(y,2)} \times \overline{n}/n_{GW}$ versus $\overline{n}/n_{GW}$ diagram (Fig. 6) shows that low triangularity plasmas with Ar seeding had 20% higher $n\tau_E$ than unseeded plasmas while ITER shaped plasmas with Ar had similar $n\tau_E$ as unseeded plasmas. Thus, Ar seeding generally allows to combine good confinement properties with high radiation levels in a mantle around the plasma. Further study is needed to reveal the physical mechanisms behind the confinement improvement with Ar in the low triangularity discharges.

4. SLOW DENSITY PROFILE EVOLUTION

For a given line averaged density and temperature profile, fusion power increases with increased peaking of the plasma density, thus optimizing the fusion yield in a reactor. Several tokamaks have observed density peaking on long time scales [23-24]. JET [25] has also recently observed similar density peaking on long time scales for various plasma currents ($0.95 \leq I_p \leq 2.5$MA) and plasma shapes. Outboard and inboard divertor fuelling as well as main chamber fuelling have been tried, with highest densities obtained when fuelling the discharge in the private region from the inboard base ring in the divertor.

Key ingredient of these experiments is the use of gas fuelling rates below the values corresponding to the degradation of the edge transport barrier. Fig. 7a. shows a plasma where the line-averaged density monotonically increased over a period of several seconds, reaching 1.1 times the Greenwald density after 5s, followed by a roll-over in confinement. Plasma density profiles illustrate the evolution from a nearly flat profile to a strongly peaked density profile at the end of discharge, with $\overline{n}/n_{ped} \sim 1.6$

At these lower heating powers ($P_{heat} < 8$MW), the current profile broadens, leading to q(0) values above 1 and the disappearance of sawtooth MHD followed by a collapse of the central temperature profile due to the accumulation of (metallic) impurities in the centre accompanied by increased core radiation. If centrally deposited ICRH is applied to avoid the loss of sawteeth, one obtains discharges with high values of the Greenwald factor (up to $\overline{n}/n_{GW} = 1.1$) but with density profiles showing a moderate peaking ($\overline{n}/n_{ped} = 1.2 - 1.3$) and reduced confinement ($H_{98(y,2)} \sim 0.6$). Higher NBI heating powers also keep sawtooth MHD but with less confinement degradation. Avoidance of MHD modes was attempted using optimized gas puff in the beginning of the discharge, usual for high δ plasmas, as explained in Sect 1. In this way discharges could be realized with a quasi-stationary phase of over 3 seconds (terminated by the end of the heating pulse) at $\overline{n}/n_{GW} = 1$, $H_{98(y,2)}=0.96$, $\beta_N=2$ with sawteeth preserved and stationary peaked density profiles with $\overline{n}/n_{ped} \sim 1.3$ (Fig. 7b). The physical mechanisms leading to the density peaking are not yet fully understood and require further study.

5. PELLET INJECTION

Pellet fueling experiments have been conducted [26] to achieve long pulse operation at densities in the vicinity of the Greenwald density with good energy confinement. A target plasma configuration with δ~0.34 and at 2.5MA/2.4T was chosen, showing a confinement collapse when trying to fuel the density beyond to $\overline{n}/n_{GW} = 0.8$ with gas puff only. Solid $4mm^3$ deuterium cubes were launched at a speed of 160m/s into the plasma from the high field side via an injection tube tilted by 44 degrees with respect to the horizontal plane and with a tangency radius at a normalised minor radius ρ~0.6-0.7. An optimised pellet fuelling scenario should minimize or avoid the following effects: (i) prompt particle losses causing too strong an increase of the neutral gas pressure and edge density, (ii) trigger of MHD activity by the pellet and (iii) ELM bursts following pellet injection. Each of these pellet related effects can cause severe energy losses from the plasma.

Mitigation of the confinement losses resulting from pellet induced ELMs was achieved with an adapted pellet fueling cycle consisting in interrupting the injected pellet string. This leads to a recovery of the plasma energy content while the particle inventory still remains high. The finally optimised pellet sequence is composed of an initial density build up phase at a pellet injection rate of about 6Hz followed by a phase where the density is sustained at an injection rate of about 2Hz. In this way, a density increase beyond the Greenwald limit was achieved without significant persistent loss of the plasma energy content, as illustrated in Fig. 8. The initial pellet sequence causes the expected energy drop due to enhanced ELM activity. The pellet string is then interrupted for about 0.5s to allow for energy recovery, followed by a string at 2Hz. With this reduced repetition rate, the transient energy drop initiated by every pellet can be almost fully recovered before the next pellet arrives in the plasma. Moreover, successive pellets gradually increase the plasma density until finally a density above the Greenwald limit is achieved with simultaneous a high plasma energy content of about 6MJ and $\beta_N > 1.8$, corresponding to a $H_{98(y,2)} \sim 0.82$. The energy and central line-averaged density of a reference discharge without gas puff or pellet injection are indicated by the dashed lines in the figure for comparison. It is clear that the discharge with the optimized pellet injection obtains the same energy content, however, at a much higher density as the nonfuelled reference. Further experiments are planned next year aimed at improving the stationarity of these discharges.

A too high pellet injection rate can lead to a severe cooling of the central plasma temperature leading to a reduction of the critical beta (because of the decrease of the ion gyroradius due to the reduction in temperature) and therefore render the plasma sensitive to the appearance of NTMs. To keep the plasma temperature sufficiently high, dominant NBI heated plasmas were also heated with centrally deposited ICRH, resulting indeed in a reduction of the MHD activity. Raising the toroidal field is also beneficial to reduce MHD, but leads for a fixed power on the contrary to type III ELMs and reduced plasma performance.

6. CONFINEMENT SCALING OF HIGH TRIANGULARITY DISCHARGES AND COMPARION OF RECENTLY OBTAINED CONFINEMENT DATA TO THE ITER DESIGN POINT PARAMETERS

(a) Influence of triangularity, density peaking and of the Greenwald factor on the enhancement factor $H_{98(y,2)}$. [27]. The new results described in the previous sections permit the investigation of the effect of triangularity and density peaking on confinement. The data obtained are compared to the standard IPB98(y,2) [2] scaling law :

$$\tau_{E,\,IPB98(y,2)} = 0.0562\, I_p^{0.93}\, B_t^{0.15}\, n^{-0.41} P^{-0.69}\, A_i^{0.19}\, R^{1.97}\, \varepsilon^{0.58}\, \kappa^{0.78}$$

with the usual units (s, MA, T, 10^{20}m^{-3}, MW, m). The residuals of the factor $H_{98(y,2)} = \tau_{E,exp} / \tau_{E,\,IPB98(y,2)}$ for a subset of the data which had accurate values of the pedestal density n_{ped} (obtained from the interferometer channel at R=3.75m in JET) have been fitted to the upper triangularity, the Greenwald factor and the density peaking factor $\bar{n}/n_{ped}$. This resulted in a corrected enhancement factor $H_{98(y,2),corr}$ defined as : $H_{98(y,2),corr} = H_{98(y,2)} * H_{cor}$. with $H_{cor} = 0.84 + 0.17\delta_U - 0.13\bar{n}/n_{GW} + 0.50$ $(\bar{n}/n_{ped} - 1)$. This expression shows clearly the increase of confinement with triangularity δ_U and density peaking $\bar{n}/n_{ped}$ and the degradation with increasing $\bar{n}/n_{GW}$. More refined expressions can be used [27], leading essentially to the same conclusion. For an illustration of the influence of density peaking on the extrapolation to ITER, we take the ITER design point (δ_U =0.5, n/n_{GW} = 0.85, $H_{98(y,2)}$ = 1). Without peaking, a confinement factor $H_{98(y,2),\,corr}$ ~ 0.81 is found. With a modest density peaking ($\bar{n}/n_{ped}$ = 1.3), this rises to $H_{98(y,2),corr}$ ~ 0.96.

(b) Comparison of confinement data to the ITER design point. The present data, reaching ITER values for $H_{98(y,2)}$ and $\bar{n}/n_{GW}$, have a 2-3 times larger normalized gyroradius ρ^*, and 10 times larger collisionality ν^* (Fig. 9a-b). Although it is not possible with JET or any existing device to reach simultaneously β, ν^* and ρ^* as in ITER, JET can generate β, ν^* and ρ^* data which are the closest to dimensionless ITER parameters. First, one can match simultaneously ITER ν^* and β_N values in JET, by operating at lower density with $\bar{n}/n_{GW}$ ~ 0.3-0.5, i.e. the normal operating density range in the absence of gas puff or pellet injection. Second, as $\rho^* \propto B^{-2/3}\, a^{-5/6}$ [2] for fixed β and ν^*, operation at high magnetic fields (together with the large machine dimensions of JET) gives the smallest ρ^* values possible at this moment in any device. Experiments on JET are needed at higher field and current to operate closer to the ρ^*_{ITER} and hence improve the preparation for the ITER operational scenario. To carry out such a programme, that is operating in excess of 4.0MA at the ITER β and ν^*, means that a total heating power in excess of 30MW will be required. It is planned that this level of power will be available towards the end of 2002.

7. ELMS IN HIGH DENSITY, HIGH CONFINEMENT PLASMAS AND POSSIBILE MITIGATION TECHNIQUES

High density, high confinement plasmas need a heat exhaust mechanism compatible with the first wall to be useful for a future fusion reactor. The power loss per ELM for ITER operating at Q=10 and 400MW fusion power, cannot be larger than ~1% of the plasma stored energy in order to avoid melting of tungsten and evaporation of carbon target materials [28]. Two effects are important when discussing the power losses by ELMS: (i) the peak power flux during the ELM itself and (ii) the power flux averaged over many ELMs. High peak power loss during ELMs can cause serious damage because of ablation and/or melting of the target material. However, for given energy loss during individual ELMs, a reduction of the ELM frequency can increase the divertor target lifetime. Several approaches are under investigation on different machines to find a solution for the power load on the first wall during ELMs : (i) the realization of so-called Type II ELMs [29-30], (ii) regimes with enhanced D_α radiation [31] and (iii) impurity seeding [10].

JET discharges at high and medium triangularity with heating powers sufficient to keep Type I ELMs show interesting properties. With increasing gas puff and corresponding increase in the edge density up to nped = 75% nGW, the frequency of the ELMs shows first a mild increase and then drops again. At extreme gas puff rates, Type III ELMs appear. Measurements show that above a pedestal density n_{ped}~75% n_{GW} the pedestal electron temperature no longer decreases with increasing pedestal electron density, but stays more or less constant and above the critical temperature for transition to Type III ELMs. In other words, the decrease of the pedestal pressure with density ($\nabla p_{ped} \propto 1/n^2$), usually seen at lower triangularity, is no longer observed in these high and medium triangularity high confinement plasmas. The net effect of the higher triangularity is thus a larger operational space for the existence of Type I ELMs at high density. First modelling attempts [32] for the edge stability with the JETTO code coupled to the infinite-n ideal ballooning stability code IDBALL [33] show second stability access for ideal ballooning for part of the edge pedestal of the plasmas at high and medium triangularity, consistent with the decrease of the Type I ELM frequency with density.

At high density ($n_{ped} > 75\% n_{GW}$) in high triangularity plasmas, broadband continuous edge-localised MHD activity is observed in between the (low frequency) ELMs. A comparison of the power input and energy loss by Type I ELMs shows that during the interval between ELMs there must be an additional energy loss channel. Under these conditions, the relative energy loss per ELM, $\Delta W_{ELM}/W_{ped}$, decreases together with the ELM frequency, which is contrary to the usual Fishpool scaling [34] in which $\Delta W_{ELM}/W_{ped}$ and the ELM frequency are approximately inversely correlated. The exact nature of the mechanism leading to these enhanced losses is a subject of further study. If power and particle exhaust can be taken over by continuous MHD activity rather than via an ELM burst, it could possibly be used to advantage for an operational scenario compatible with the first wall.

The various observations on ELM behaviour with pellet injection, impurity seeding, high and medium triangularity discharges with Type I ELMs can be summarized in a unique relationship

between the relative energy loss per ELM ($\Delta W_{ELM}/W_{ped}$) and the collisionality in the pedestal before the ELM burst, ν^*_{ped}, showing a decrease of the relative ELM losses as a function of ν^*_{ped} [35] (Fig. 10). However, this experimental fact could also be attributed to the dependence of MHD on the pedestal collisionality or to other processes associated with the relative duration of the phase of enhanced MHD activity and the characteristic time of the parallel energy loss, depending in different ways on collisionality. According to the exact mechanism, the extrapolation of these results to ITER can differ substantially.

Measurements of power deposition profiles (averaged over ELMs) on the divertor target plates in discharges at 2.5MA/2.4T in JET and heated with 12MW of NBI shows that the peak heat flux was strongly reduced (from 20 to 4 MW/m^2) in discharges at higher densities obtained with D_2 puff [36]. This reduction in the peak power load is observed because of the disappearance of the so-called 'narrow feature' in the power load profile on the target [35] indicating a decrease of the fast ion losses from the edge plasma and is possibly further enhanced by a decrease of the peak power load during the ELM.

Summarizing, medium and high triangularity high density, high confinement plasmas without impurity seeding and with Type I ELMs show the following interesting ELM properties : (i) an ELM frequency which remains low even at high gas fuelling rates, (ii) the relative losses per ELM $\Delta W_{ELM}/W_{dia}$ which do not increase with decreasing ELM frequency (iii) an ELM average power flux which decreases with increasing fuelling. In impurity seeded discharges, the presence of the impurity not only increases radiation, but also changes the character of the ELMs [18, 34]. In low triangularity discharges, a difference has been observed in the effect of the impurity on the character of the ELMs both during the D_2 puff phase and during the afterpuff. Impurity seeding (by Ar or Ne) applied during the main D_2 puff phase can change the ELMs from Type I to more benign high frequency Type III ELMs, but with reduced confinement. Impurity seeding applied in the afterpuff reduces the frequency of Type I ELMs, and can, with excessive Ar seeding lead to intermittent ELM-free phases, and a tendency to impurity accumulation [13].

In high triangularity discharges with adequate impurity seeding not only the ELMs remain of Type I, but they are also reduced in frequency. Also in this case $\Delta W_{ELM}/W_{dia}$ does not follow the usual Fishpool scaling [36] at low frequency, and is reduced by a factor of about 5 [34]. This is consistent with the infrared thermographic measurements, indicating a dramatic drop in the peak and base level temperature in the inner and even more in the outer divertor (Fig. 5b). Although the estimates of ELM power loss from the profiles indicate values on the order of 2.5% of the stored energy [18], it is still unresolved where and in what way the lost power arrives at the first wall. Part of it could well be radiated away before arriving at the target plates where the plasma is possibly in a partial detachment state. However, the extrapolation of this ELM buffering effect has to be further confirmed experimentally, as modelling [28] seems to indicate that with increasing ΔW_{ELM} the

mitigation effect by radiation could be less efficient. These questions will be adressed in coming campaigns. In any case, the results obtained up to now show that impurity seeding is an important tool to influence the ELM frequency and amplitude independent of the triangularity of the plasma [34].

8. MHD IN HIGH DENSITY HIGH CONFINEMENT PLASMAS

NTMs often limit the performance of high density, high confinement discharges on JET. Dedicated experiments have demonstrated that NTMs are metastable in standard q_{95}~3.4 scenarios as soon as the discharge is in H-mode. Furthermore, at the crash of long sawtooth periods, NTMs can be destabilized at low β_N values. On the contrary, reducing the amplitude of the sawteeth reduces the chance to destabilize NTMs, leading to higher β_N values before the mode sets in. Therefore specific scenarios have been developed to avoid plasma perturbations (sawteeth with a large sawtooth period, large first ELMs or pellets) which could destabilise NTMs. This has especially been beneficial for the high triangularity, high confinement studies [8,9], but also for the experiments with density peaking on long time scales [25]. The role and the need for a control of large sawteeth in inducing NTMs in discharges has been shown in Ref. [37] in particular in relation to discharges with ICRH.

3/2 modes deteriorate the performance of standard scenarios, and 2/1 modes lead to a disruption. The higher m/n=5/4 and 4/3 modes are usually destabilised before the 3/2 modes and have therefore a lower threshold or the island needed to trigger these modes is more easily generated. They are not as detrimental as the 3/2 modes as they are located more towards the plasma centre. However, for the experiments with density peaking, which are more prone to NTMs due to the steep density profiles leading to a nonnegligible bootstrap current fraction of 16-20%, they are important as they stop the monotonic increase of the central density.

CONCLUSIONS AND FUTURE WORK.

Over the last year plasmas have been realised in JET with high confinement $H_{98(y,2)} \sim 1$ at high densities $\bar{n}/n_{GW} \sim 1$. This has been possible by (i) increasing the average triangularity of the plamas, up to δ~0.5, and has been extended to plasmas with medium triangularity $\delta \sim 0.3$-0.4 by increasing the heating power such as to sustain Type I ELMs (ii) in low and high triangularity plasmas using impurity seeding, showing on top of the good confinement properties high radiated power fractions (up to 70%) and (iii) by plasma fuelling with an optimised pellet timing sequence, allowing sufficient time between the successive pellets for the plasma energy to recover without losing too much the density. Furthermore, experiments showed (i) the importance of central heating to maintain sawtooth MHD, preventing impurity accumulation (ii) the influence of the deuterium gas puff rate in obtaining high confinement and density peaking and (iii) the importance of Ar seeding to create a radiating belt and to contribute to the mitigation of ELMs. These techniques allowed JET (Fig. 11) to reach the ITER Q=10 requirements. Moreover, two factors can lead to the decrease of the power load on the target plates : impurity seeding and high triangularity plasmas with broadband inter-ELM MHD activity.

The insights gained, the techniques learned and the data obtained this year are important steps towards ITER. Nevertheless, further work is needed to understand the physics of ELMs at high density and with impurity seeding, and from there to improve the mitigation of ELMs, to extend the stationarity of the plasmas, study the influence of the different heating methods on confinement and ELM behaviour, to mention but a few. In addition, an extension of the results obtained to higher currents, fields and heating powers is necessary to improve the extrapolation of the different high performance regimes to ITER.

ACKNOWLEDGEMENTS

It was a great pleasure to share the work with all the European and non-European colleagues at JET this year. The excellent work done by the colleagues from UKAEA responsible for the operation of JET, has been an important factor in the succes of the 2000-2001 experimental campaigns. The work described in this paper has been performed under EFDA (European Fusion Development Agreement).

REFERENCES

[1]. M. Greenwald et al., Nucl. Fusion, 28, 2199 (1988)
[2]. ITER Physics Basis, Nucl. Fusion, 39, 2175 (1999)
[3]. J. Stober et al., Plasma Phys. Contr. Fusion 42, A211 (2000); W.Suttrop et al., Plasma Phys. Contr. Fusion 42, A97 (2000)
[4]. T.H. Osborne et al., Plasma Phys. Contr. Fusion 42, A175 (2000)
[5]. G. Saibene, L.D.Horton, R.Sartori et al., Nucl. Fusion, 39, 1133 (1999)
[6]. P.J. Lomas et al., Plasma Phys. Contr. Fusion 42, B115 (2000)
[7]. Y. Kamada et al., Fusion Energy 1996 (Proc. 16th Conf. Montreal, 1996), Vol 1, IAEA, Vienna (1997) 247
[8]. R. Sartori, this conference, contribution P3.003
[9]. G. Saibene, this conference, Contribution P3.002
[10]. J. Ongena et al., Plasma Physics 8, 2188 (2001)
[11]. J.D. Strachan et al., Plasma Phys. Contr. Fusion 42, A81 (2000)
[12]. P. Dumortier, this conference, contribution P3.004
[13]. M.E. Puiatti, this conference, contribution P3.007
[14]. M. Nave, this conference, contribution P3.009
[15]. H.R. Koslowski, this conference, contribution P3.010
[16]. G. Jackson, this conference, contribution P3.017
[17]. M. Tokar', this conference, contribution P3.032
[18]. S. Jachmich, this conference, contribution P3.013
[19]. L. Horton et al., Controlled Fusion and Plasma Physics, Proc. 26th EPS Conf., Maastricht 1999, paper P1.021

[20]. J. Ehrenberg et al., “Wall effects on particle recycling in tokamaks” published in “Physical Processes of the Interaction of Fusion Plasmas with Solids” (Academic Press, 1996).
[21]. J. Ongena, M. Evrard, D. Mccune, Fusion Technology 37, 313 (2000)
[22]. Th. Eich, this conference, contribution P5.010
[23]. M.A. Mahdavi et al., Proc. 18th IAEA Fusion Energy Conference (4-10 Oct. 2000, Sorrento, Italy) paper IAEA-CN-77/ EXP1/04
[24]. J. Stober, 8th European Fusion Physics Workshop, Leysin 13-15 December 2000
[25]. M. Valovic, this conference, contribution P3.008
[26]. P.T. Lang, this conference, contribution P3.012
[27]. G. Cordey et al, this conference, contribution P3.011
[28]. A. Loarte, Proc. 18th IAEA Fusion Energy Conference (4-10 Oct. 2000, Sorrento, Italy) paper IAEA-CN-77/ ITERP/11(R)
[29]. Y. Kamada et al., Plasma Phys. Contr. Fusion 42, A247 (2000)
[30]. J. Stober, M. Maraschek et al., Nucl. Fusion 41, 1123 (2001)
[31]. M. Greenwald et al., Phys. Plasmas 6, 1943 (1999)
[32]. V. Parail, this conference, contribution P5.027
[33]. T. Hender, UKAEA Fusion, Association “UKAEA-Euratom”, private communication.
[34]. G.M. Fishpool, Nucl. Fusion 38, 1373 (1998)
[35]. A. Loarte, this conference, contribution P3.005
[36]. W. Fundamenski et al., this conference, contribution P4.073
[37]. O. Sauter et al, this conference, contribution P5.001

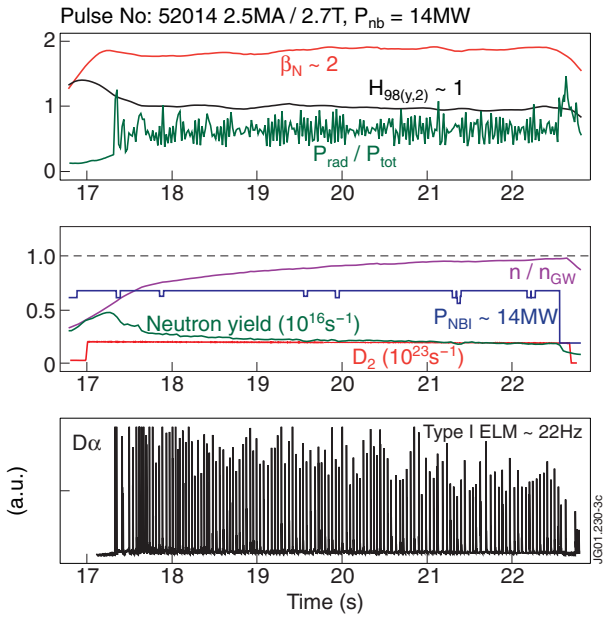

Figure 1: Time traces of an ITER-like JET plasma (Pulse No: 52014, 2.5MA/2.7T) obtained at high triangularity (δ~0.47) showing simultaneously realization $\bar{n}/n_{GW} > 0.85$, $\beta_N \sim 2$ and $H_{98(y,2)} \sim 1$ from about t=20s onwards.

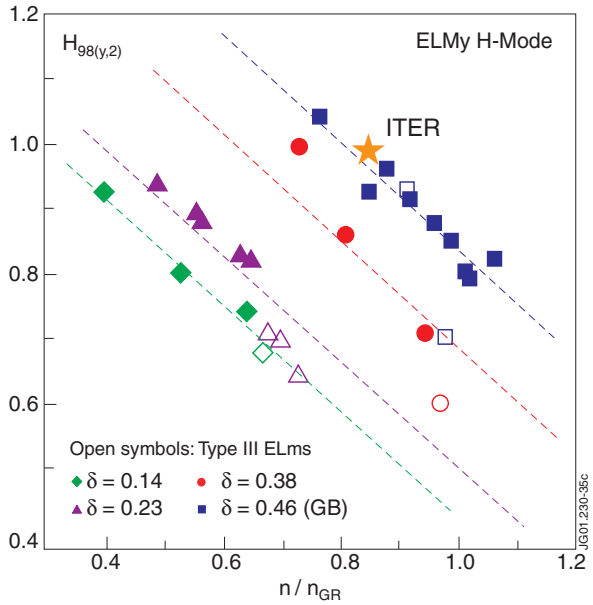

Figure 2: Plot of the enhancement factor $H_{98(y,2)}$ versus the Greenwald factor n/n_{GW} in discharge series with different triangularities and no impurities. Data for δ up to 0.38 have been obtained in the MkII JET divertor [9]. The highest triangularity data ($\delta = 0.46$) have been obtained this year in the gasbox divertor (MkIIGB) configuration. The projected ITER design point is indicated by the star. Open symbols correspond to discharges with Type III ELMs.

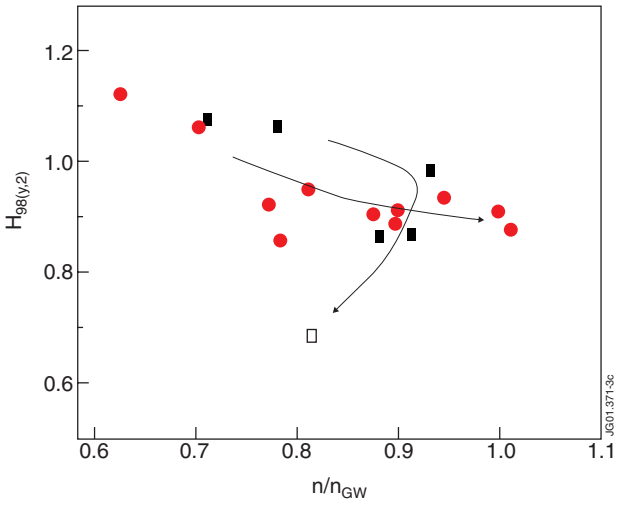

Figure 3: The enhancement factor H98(y,2) for medium triangularity plasmas (δ~0.3) as a function of the Greenwald number. Circles correspond to discharges at 1.9MA/2.0T with $P_{heat}/P_{L-H} > 2.4$, squares to discharges at 2.4MA/2.4T and 1.9MA/2.0T with $1.6 < P_{heat}/P_{L-H} < 2.4$. Open symbols indicate Type III, solid symbols Type I ELMs. Arrows show the direction of increasing gas puff rates. For the second class of discharges, confinement and density is reduced at high gas puff rates, accompanied by the appearance of Type III ELMs.

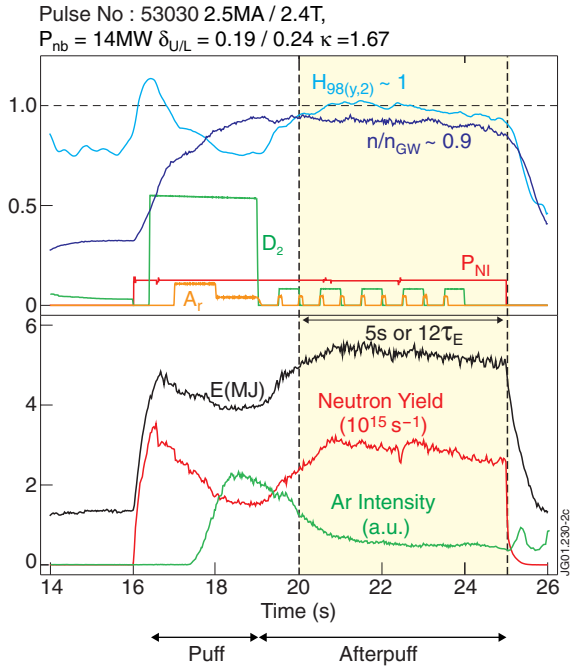

Figure 4: Ar seeding in a low triangularity (δ~0.22) ELMy-H Mode plasma with the Xpoint on the septum. Time evolution of the enhancement factor $H_{98(y,2)}$, the Greenwald factor, neutron yield, plasma stored energy, bulk radiation and deuterium and Ar injection rate. The main puff phase consists of D and Ar injection, intended to increase both the density and radiation level in the discharge. The "afterpuff" phase (with reduced levels for D_2 and Ar puff) had simultaneous high confinement and high density.

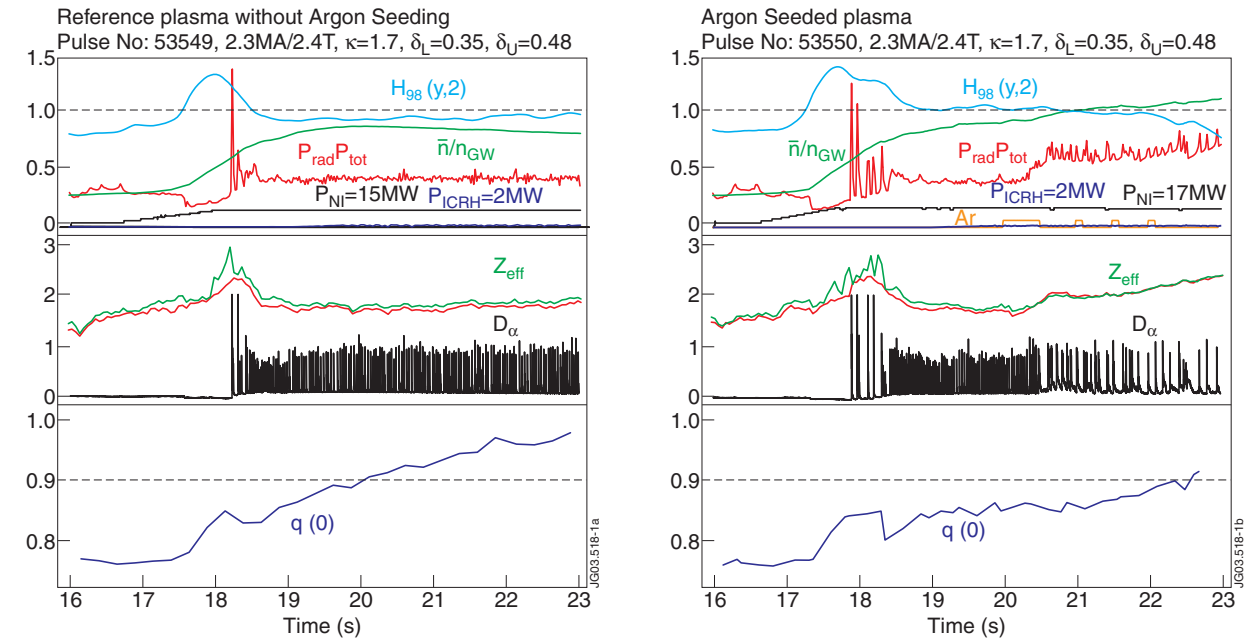

Figure 5:(a) Ar seeding in a high triangularity (δ~0.47) ELMy-H Mode plasma. Temporal evolution of confinement parameters, central q value, D_α intensity and Z_{eff}. The nonseeded reference plasma (left, Pulse No: 53549) and plasma with Ar seeding (right, Pulse No: 53550) were both NBI heated (15MW, resp. 17MW) with additional 2MW of centrally deposited ICRH (H-minority heating). Ar seeding in Pulse No: 53550 started at t=20s, and radiation fractions P_{rad}/P_{tot} ~ 70% were achieved.

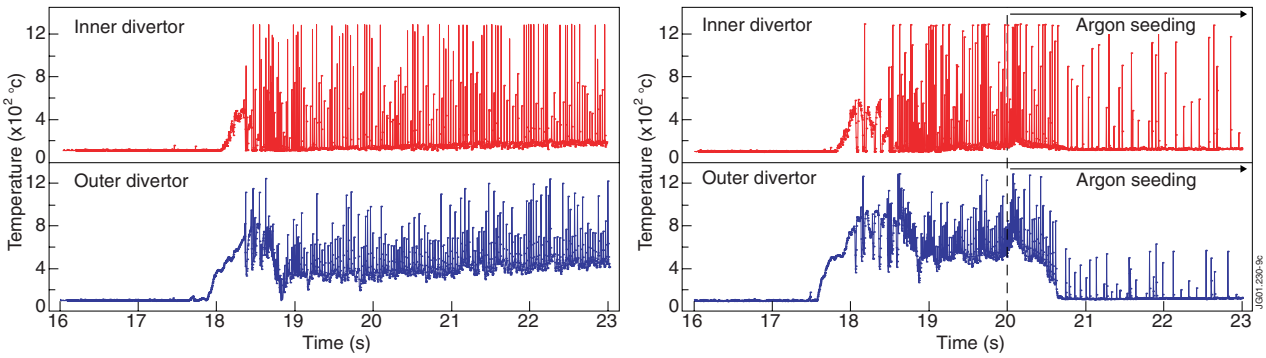

Figure 5:(b) Infrared measurements of the JET divertor target plates for the same discharges as Fig 5a.

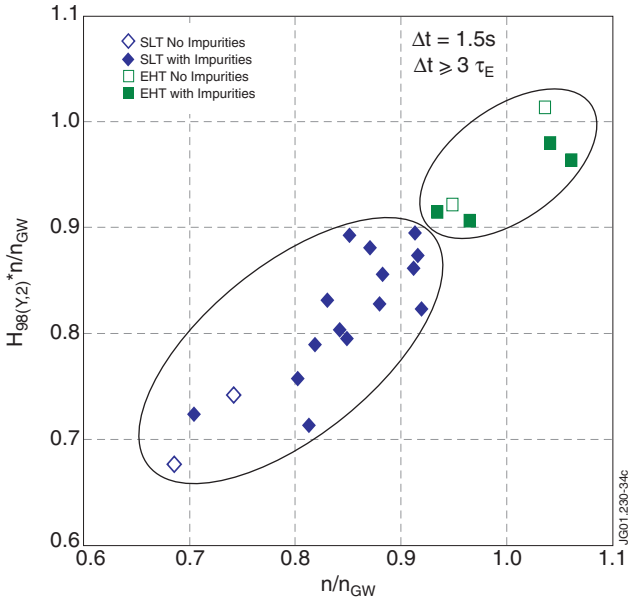

Figure 6: Confinement plotted versus Greenwald number for Ar seeded plasmas (solid symbols) and reference cases (open symbols). Values are obtained by averaging over time intervals of 1.5s (about $3\tau_E$ for the discharges considered). Data belong to two distinct discharge types : (i) with X-point on the septum at low δ=0.15 (diamonds), and (ii) ITER-like discharges at high δ=0.45 (squares).

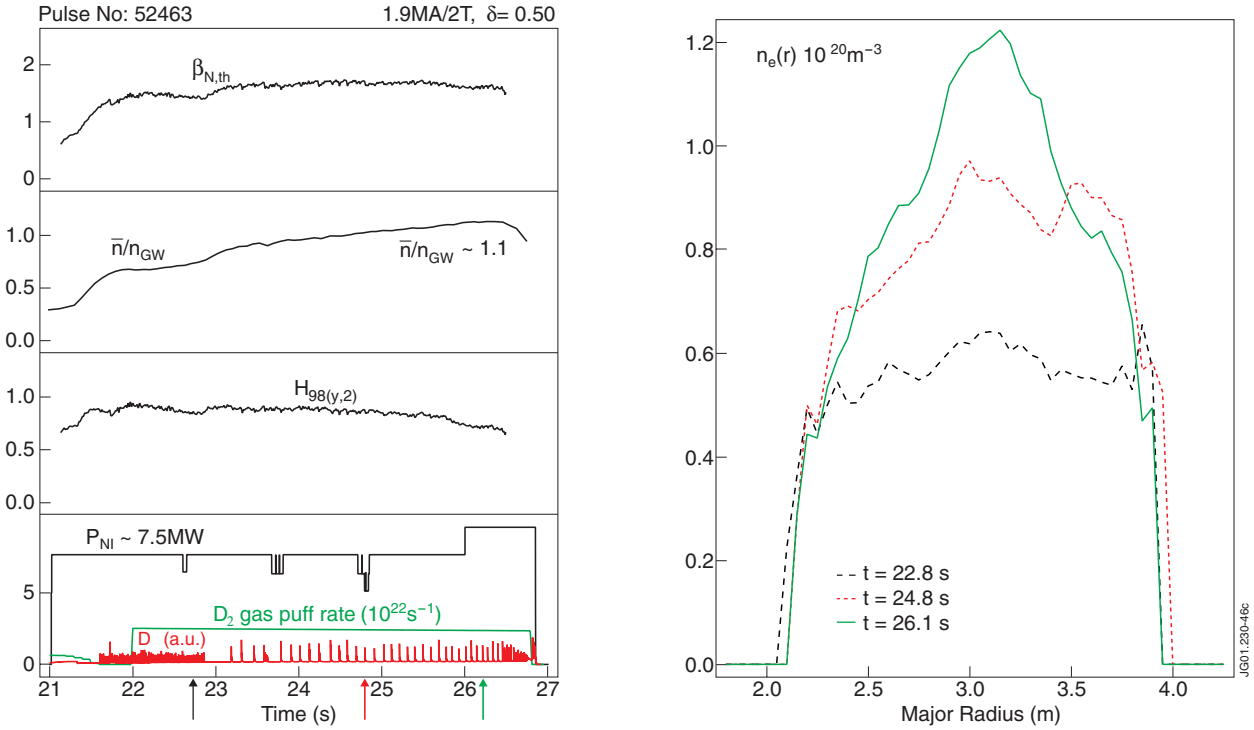

Figure 7:(a) Time evolution and density profiles of a high triangularity (δ=0.5) discharge with spontaneous density peaking, heated with 7.5MW of NBI. Careful gas puff is applied, leading to values of the density up to $\bar{n}/n_{GW}$ ~ 1, at nearly constant values for β_N ~ 1.7, but with a slightly degrading $H_{98(y,2)}$ with increasing density. Density profiles are shown for the times indicated by the arrows.

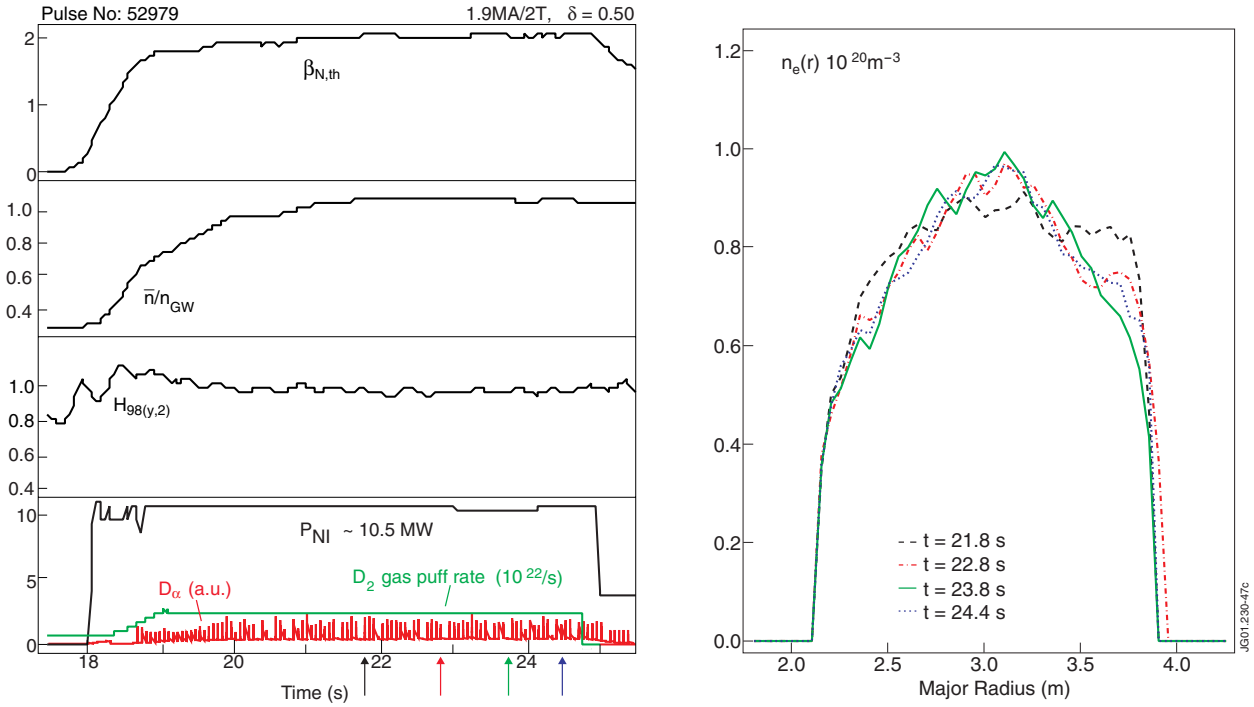

Figure 7b : Time evolution and density profiles of a high triangularity (δ=0.5) discharge with spontaneous density peaking, heated with 10.5 MW of NBI. Gas puff is applied, leading to values of the density up to n/n_{GW}~ 1, at nearly constant values for β_N ~ 2 and $H_{98(y,2)}$ ~ 1. Density profiles are shown for the times indicated by the arrows.

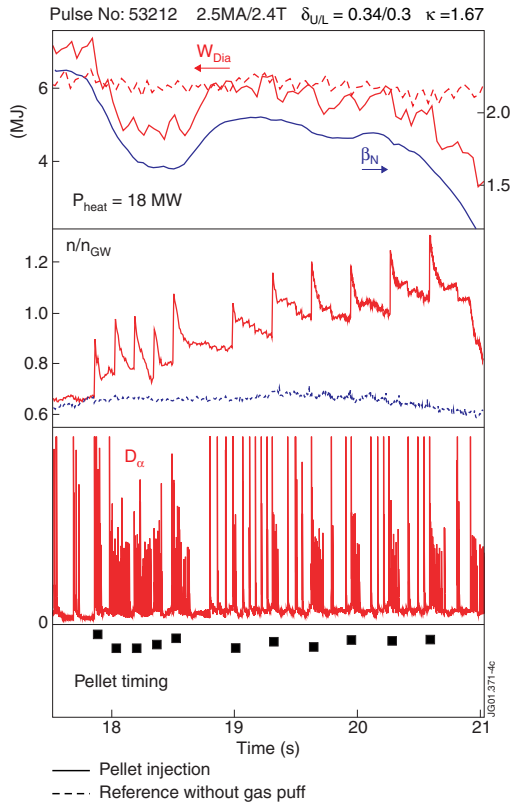

Figure 8: Time evolution of the diamagnetic energy, normalized beta, Greenwald factor and the intensity of the D_α line for a medium triangularity JET discharge with an optimised pellet fuelling cycle. Squares indicate the timing sequence of the pellets. Solid lines correspond to the discharge with pellets, dashed lines to a reference discharge without gas puff.

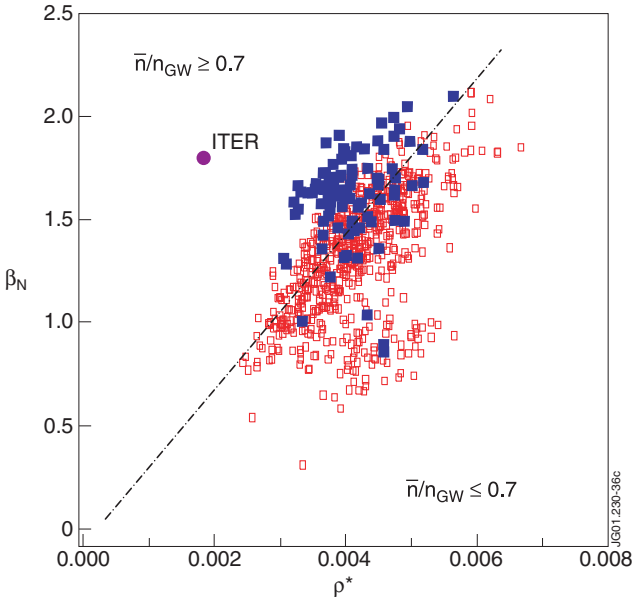

Figure 9(a) Normalized β_N plotted versus normalized gyroradius ρ^* for JET ELMy HMode discharges since 1994 with 1.8MA < I_p < 2.7MA. Data are from the JET steadystate database. Open symbols correspond to data obtained before 2000, solid symbols to those from 2000-2001. The dashed-dotted line roughly divides this diagram in a region below and above $\bar{n}/n_{GW}$ = 0.7. The ITER design point is indicated by the solid circle.

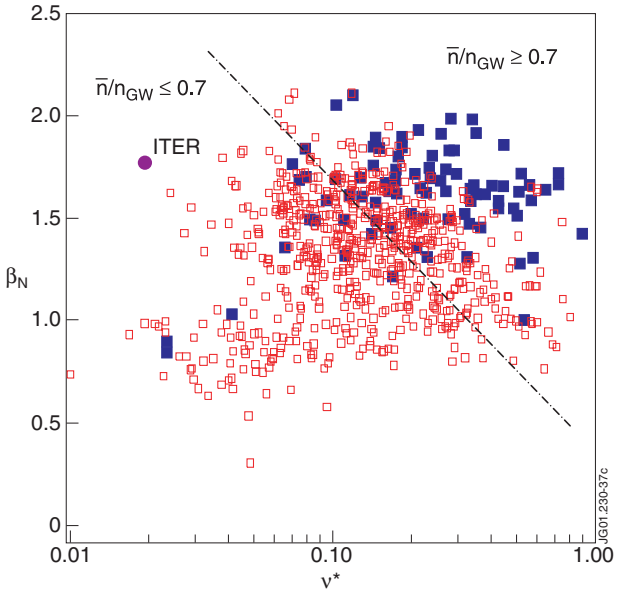

Figure 9:(b) Normalized β_N plotted versus collisionality ν^* for JET ELMy H-Mode discharges since 1994 with 1.8MA < I_p < 2.7MA. Data are from the JET steady-state database. Open symbols correspond to data obtained before 2000, solid symbols to those from 2000-2001. The dashed-dotted line roughly divides this diagram in a region below and above $\bar{n}/n_{GW}$ = 0.7. The ITER design point is indicated by the solid circle.

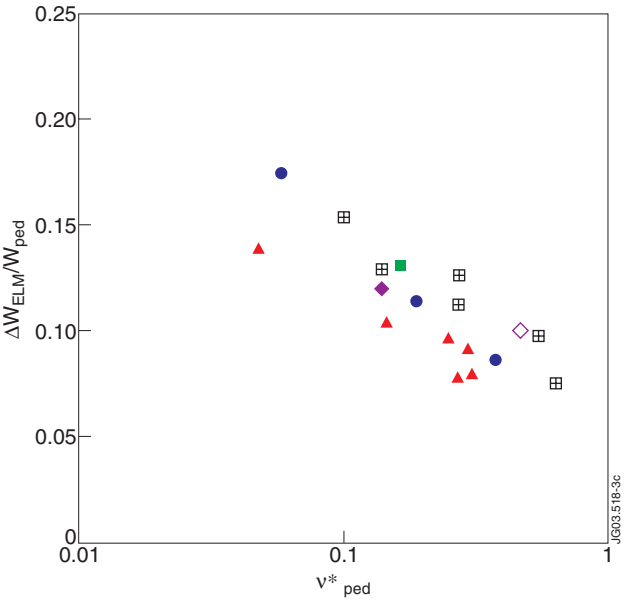

Figure 10: Relative ELM losses $\Delta W_{ELM}/W_{ped}$ plotted versus edge pedestal collisionality ν^*_{ped}, for several discharges in JET (circles : medium triangularity discharges δ~0.33 at 2.5MA/2.7T; squares : medium triangularity discharges δ~0.33 at 2.5MA/2.7T with pellet injection; crossed squares : high triangularity δ~0.5 at 2.5MA/2.7T; up triangles : medium triangularity discharges δ~0.33 at 1.9MA/2.0T; full diamonds : low triangularity δ~0.2 Ar seeded discharges at 2.5MA/2.4T, open diamonds : high triangularity δ~0.5 Ar seeded discharges at 2.5MA/2.7T).

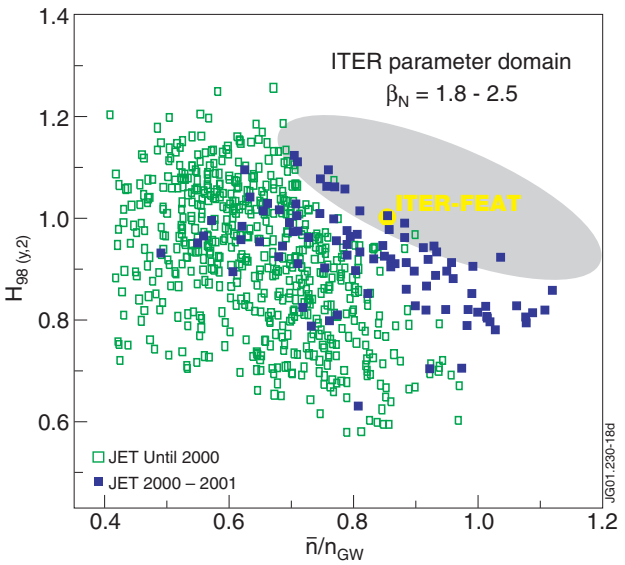

Figure 11: Confinement $H_{98(y,2)}$ plotted versus the Greenwald factor $\bar{n}/n_{GW}$ for JET ELMy H-Mode discharges since 1994 with 1.8MA < I_p < 2.7MA. Data are from the JET steadystate database. Open symbols correspond to data obtained before 2000, solid symbols to those from 2000-2001. The full circle corresponds to the ITER working point. The shaded zone corresponds to the ITER parameter domain with 1.8 < β_N < 2.5.